Dynamics of Atmospheres and Oceans 85 (2019) 57–71

Contents lists available at ScienceDirect

Dynamics of Atmospheres and Oceans

journal homepage: www.elsevier.com/locate/dynatmoce

Response of ocean dynamics to multiple equilibria of the Kuroshio path South of Japan

Libin Ma[a,b,c]

[a] Key Laboratory of Meteorological Disaster of Ministry of Education (KLME)/Joint International Research Laboratory of Climate and Environment Change (ILCEC)/Collaborative Innovation Center on Forecast and Evaluation of Meteorological Disasters (CIC-FEMD), College of Atmospheric Science, Nanjing University of Information Science and Technology, Nanjing, 210044, China
[b] Earth System Modeling Center, College of Atmospheric Science, Nanjing University of Information Science and Technology, Nanjing, 210044, China
[c] China-US joint Atmosphere-Ocean Research Center and International Pacific Research Center, School of Ocean and Earth Science and Technology, University of Hawaii at Manoa, Honolulu, Hawaii, 96822, USA

ARTICLE INFO

Keywords:
Kuroshio paths
Eddy kinetic energy
potential vorticity
relative vorticity
eddy-mean flow interaction
stability analysis

ABSTRACT

Variability of the Kuroshio path to the south of Japan plays a central role in the local climate change and exerts tremendous influences on the local atmosphere and ocean. In this study, the response of ocean dynamics, in terms of the eddy kinetic energy (EKE), potential vorticity (PV), relative vorticity, and eddy-mean flow interaction, to the Kuroshio path change is discussed. Kuroshio path south of Japan includes the near-shore non-large meander (nNLM), the off-shore non-large meander (oNLM), and the typical large meander (tLM). Analyses reveal that the distribution of EKE, PV, relative vorticity, and energy exchange between the eddy field and the mean flow respectively varies with the Kuroshio path: (1) The tLM has the maximum EKE along the path; (2) The positive and negative PV are located at the onshore and offshore side of Kuroshio axis, respevetively; (3) The distributions of anomalous relative voritcity of nNLM, oNLM, and tLM are consistent with sea surface height anomalies (SSHAs); (4) The tLM has the largest energy exchange between the eddy field and the mean flow in terms of the rate of barotropic energy conversion. On the other hand, the stability analysis of ocean currents suggests that the three Kuroshio paths south of Japan have their own intrinsic properties of the instability.

1. Introduction

As a typical western boundary current, Kuroshio exhibits multi-modes in the ocean south of Japan. It usually takes three paths: near-shore non-large meander (nNLM), off-shore non-large meander (oNLM), and typical large meander (tLM) (Kawabe, 1995). Due to its northward transport, Kuroshio carries large amount of heat from low latitudes to high latitudes and significantly influences the water budget of wind-driven circulation. On the other hand, extensive mesoscale eddies generated with the variability of Kuroshio path attribute to the dynamic instability; meanwhile, they are also used to account for the meridional heat transport (Hall, 1991). Moreover, tLM of Kuroshio path has profound influence on the extratropical cyclone and storm activities (e.g,Nakamura et al., 2013; Hayasaki et al., 2013) and the biogeochemical processes (e.g., Nakata et al., 1994; Miyamoto et al., 2017). Thus, it is important to understand how the energy exchange and interaction between the mean flow and the eddy field reacts to the changes in Kuroshio paths South of Japan.

Since the high-quality satellite dataset of sea level is available, many studies have addressed that the mesocale eddies play a

E-mail address: malibin109@gmail.com.

https://doi.org/10.1016/j.dynatmoce.2019.01.001
Received 28 December 2017; Received in revised form 29 November 2018; Accepted 2 January 2019
Available online 03 January 2019
0377-0265/ © 2019 Elsevier B.V. All rights reserved.

significant role in the transitions among Kuroshio paths (Ebuchi and Hanawa, 2000, 2003; Mitsudera et al., 2001; Miyazawa et al., 2004). By analyzing the satellite data, Mitsudera et al. (2001) and Waseda et al. (2003) concluded that the formation of meander path of Kuroshio is related to the anticyclonic eddies propagated from the Kuroshio Extension. As these eddies are transported to the southeast of Kyushu, they interact with the Kuroshio currents, triggering a small meander locally. Subsequently, the small meander is propagated downstream along Kuroshio currents, further exciting the formation of the meander path of Kuroshio south of Honshu. To verify this, an anticyclonic eddy is artificially introduced in the ocean models to discuss the mechanism of the Kuroshio path transition from nNLM to oNLM or tLM (Akitomo and Kurogi, 2001; Endoh and Hibiya, 2001; Miyazawa et al., 2004; Usui et al., 2008). On the other hand, some studies explored the interaction between the mean flow and the mesoscale eddies using the data of satellite altimeter. Qiu and Chen (2010a) pointed out the interaction between mean flow and mesoscale eddies can modulate the decadal variation of the Kuroshio Extension. Their results showed the cyclonic eddies affect the trough of meander of the Kuroshio extension and anticyclonic eddies exert influence on the ridge of meander of the Kuroshio extension.

Although there are a lot of concerns on the characteristics of the mesoscale eddies and their impact on the Kuroshio south of Japan, the interaction between the eddy field and the mean flow and the stability of ocean currents responding to different Kurshio paths have not been systematically elaborated. Following the work of Ma and Wang (2014), which discussed the interannual variation of energy conversion and interaction between the mesoscale eddies and the mean flow in the Kuroshio south of Japan, the main purpose of this study is to statistically explore the ocean response to changes in the Kuroshio paths.

The rest of this study is arranged as follows. The dataset and the corresponding processing methods are addressed in section 2. Section 3 briefly introduces the classification and basic characteristics of the Kuroshio paths. The response of ocean dynamics, including the eddy-mean flow interaction and the stability of ocean currents, to Kuroshio paths is also discussed in section 3. The summary and discussion are followed in section 4.

2. Data and processing methods

The datasets used in this study include the satellite altimetry and subsurface temperature and salinity. The 19-year data spans from 1993 to 2011. The satellite altimeter is the gridded-merged anomalous sea surface height (SSH) provided by AVISO (Ducet et al., 2000; Le Traon et al., 2003; AVISO, 2008; http://www.aviso.oceanobs.com). The spatial and temporal resolutions of SSH are $1/3^\circ \times 1/3^\circ$ and 7 days, respectively. The subsurface temperature and salinity data has a horizontal resolution of $1^\circ \times 1^\circ$ and there are 24 vertical levels with the deepest depth of 1500 m (Ishii et al., 2003, 2005, 2006; named as Ishii's subsurface temperature and salinity data). They are downloaded from the University Corporation for Atmospheric Research (UCAR).

2.1. Definition of the Kuroshio axis

Due to surface heat flux, the steric height caused by the thermal expansion of the upper sea water is included in the variation of SSH. Moreover, the semiannual and annual variations of SSH south of Japan are mainly explained by the steric height (Ma, 2014). To focus on the dynamic aspects of the Kuroshio, the biannual and annual components are removed from the anomalous SSH using the harmonic analysis (Zhang and Ichikawa, 2005). Thus, a SSH dataset is reconstructed in this study by adding the mean dynamic topography data (Rio et al., 2011) to the resulted anomalous SSH. There are several methods applied to define the Kuroshio axis, such as the use of an isoline of SSH (e.g., Qiu and Chen, 2005) and the maximum velocity (e.g., Yan et al., 2016; Chang et al., 2018). In this study, two methodologies are compared to define the Kuroshio path: One is using a specific isoline and the other is using the maximum gradient of SSH. Fig. 1a shows the 115-cm isoline (white curve) and the axis defined by maximum gradient of SSH (red curve). It illustrates that the 115-cm isoline well matches the positions of the maximum meridional gradient of SSH. On the other hand, the 115-cm isoline smoothly depicts the main axis of Kuroshio path south of Japan. Thus, the 115-cm isoline is chosen to represent the Kuroshio axis in this study. After locating the position of Kuroshio axis, a time series recorded the latitudinal information of Kurshio axis is determined at each longitude, which is used to distinguish the different Kuroshio paths south of Japan.

2.2. Basic calculations

The decomposition of a field is introduced firstly. Assuming that a physical variable A has N discrete samples and varies with time, A can be divided into the time-mean flow, which is independent of the time, and a disturbance, which varies swiftly with the time (e.g., Berloff and Meacham, 1998; Ma and Wang, 2014), as follows:

$$A(x, y, t) = \overline{A(x, y)} + A'(x, y, t) \tag{1}$$

where $\overline{A(x, y)} = \frac{1}{N}\sum_{i=1}^{N} A(x, y, t)$, $A'(x, y, t) = A(x, y, t) - \overline{A(x, y)}$, and $A'(x, y, t)$ satisfies $\overline{A'(x, y, t)} = \frac{1}{N}\sum_{i=1}^{N} A'(x, y, t) = 0$. In this study, variable A can be the SSH or the zonal and meridional components of geostrophic flow. Note that A' consists of the intraannual and interannual variations in this study.

The geostrophic flow is calculated by the following relationship of geostrophic balance:

$$u_g = -\frac{g}{f}\frac{\partial h}{\partial y}, \quad v_g = \frac{g}{f}\frac{\partial h}{\partial x}, \tag{2}$$

where (u_g, v_g) are the zonal and meridional components of geostrophic flow, h is the SSH, g and f are the gravitational acceleration and Coriolis parameter, respectively. Furthermore, the eddy kinetic energy (EKE) is calculated by:

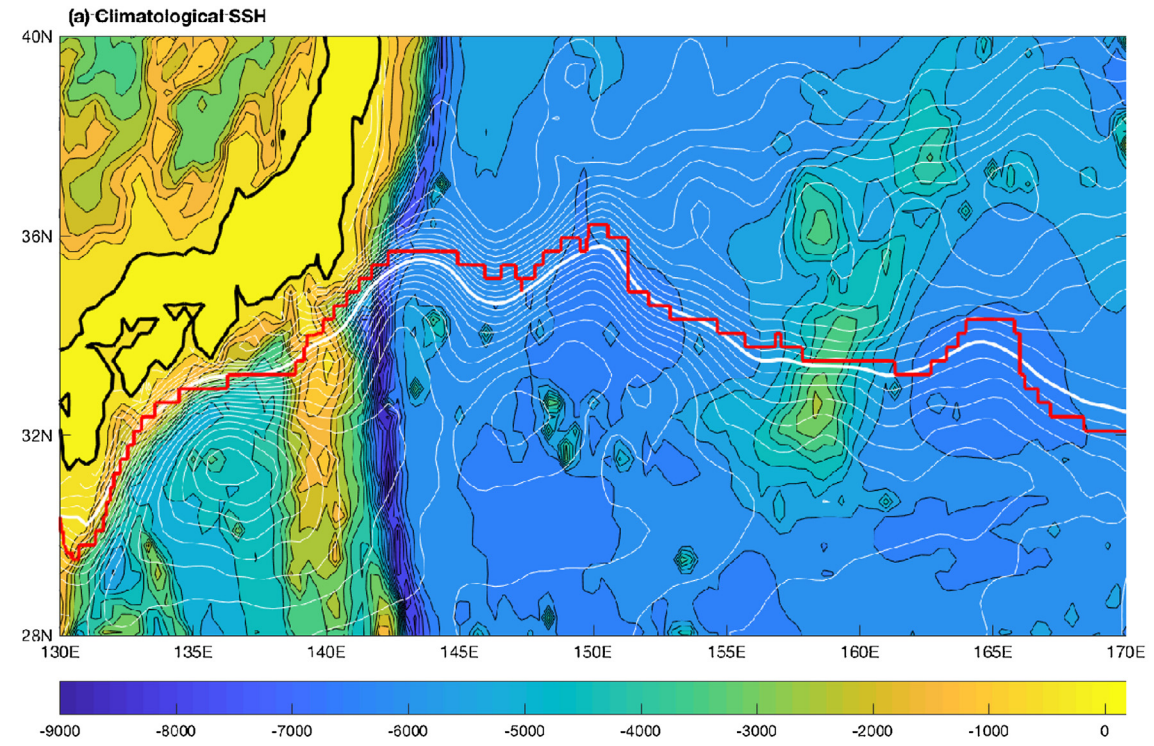

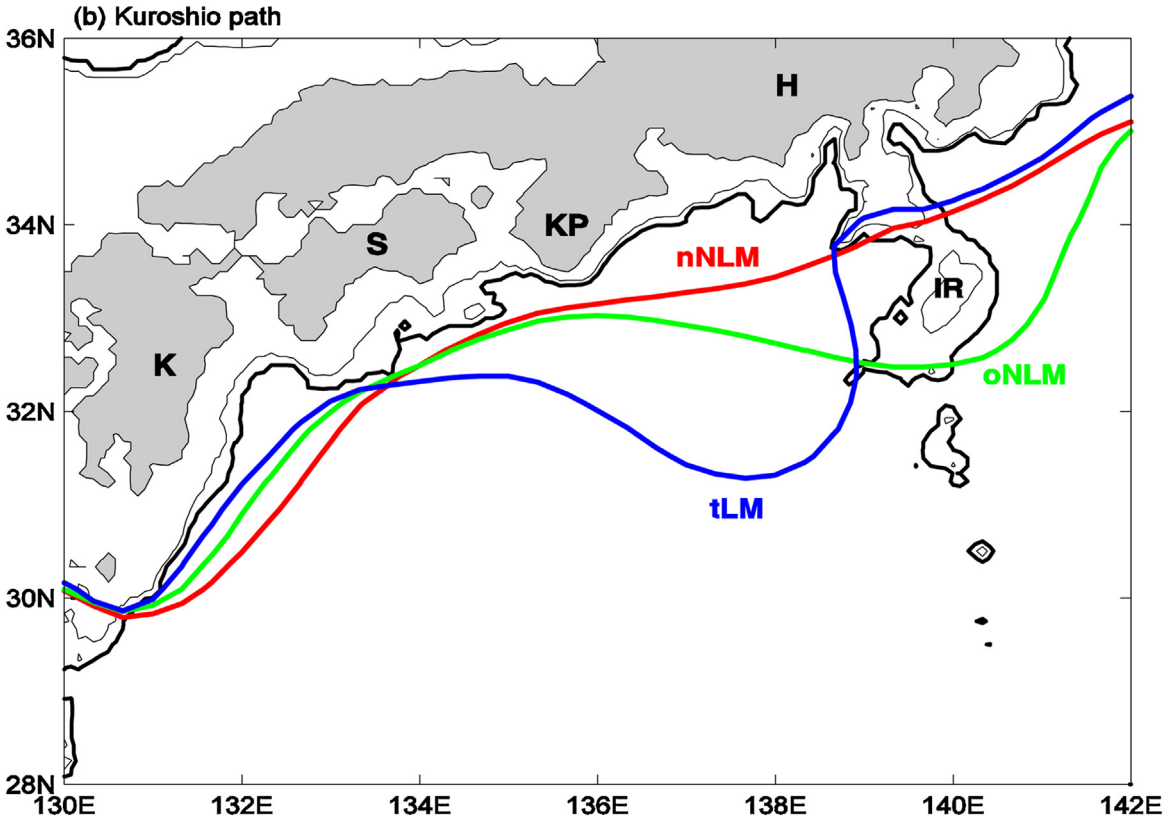

(caption on next page)

Fig. 1. (a) Climatological mean sea surface height (SSH) (1993-2011) reconstructed from the altemetric SSH anomaly data and mean dynamic topography data. The contour interval (CI) is 5 cm. The thick white line indicates he axis of the Kuroshio and its extension, which is defined as the 115-cm SSH isoline. The thick red curve represent the Kuroshio defined by the maximum SSH gradient. Shading denotes the bathymetry features from ETOPO5 (unit is m). (b) Three typical paths of the Kuroshio south of Japan. Labels 'tLM', 'nNLM', and 'oNLM' in (b) represent the typical large meander, nearshore non-large meander, and offshore non-large meander, respectively. 'K', 'S', 'KP', 'H', and 'IR' in (b) denote Kyushu, Shikoku, Kii peninsula, Honshu, and Izu Ridge, respectively.

$$EKE = \frac{1}{2}\langle u'^{2}_{g} + v'^{2}_{g}\rangle \tag{3}$$

Where $\langle \bullet \rangle$ represents the 5-week running mean; u'_g and v'_g are the zonal and meridional components of anomalous geostrophic flow, respectively. And the potential vorticity (PV) is defined as:

$$Q = \frac{f+\zeta}{\rho_0}\nabla_z \rho_\theta \tag{4}$$

where $\varsigma = \frac{\partial v_g}{\partial x} - \frac{\partial u_g}{\partial y}$ is the relative vorcitiy, ρ_0 is the reference density, ρ_θ is the potential density, and ∇_z is the operator of vertical gradient.

2.3. Classification of the Kuroshio path and observed statistics

Similar to the definition of Sugimoto and Hanawa (2012), combining the features of Kuroshio path south of Japan, Kuroshio path is distinguished by the following criteria in this study:

(1) A Kuroshio path belongs to the type of nNLM, if the mean of Kuroshio axis averaged over 135 °E~136 °E and 137 °E~138 °E locates north of 32 °N and 33.1 °N, respectively, and the Kuroshio axis along 140 °E locates north of 40 °N;
(2) A Kuroshio path belongs to oNLM, if the mean of its axis averaged over 135 °E~136 °E locates north of 32 °N, and its axis along 140 °E locates north of 33.2 °N;
(3) A Kuroshio path belongs to tLM, if its mean averaged over 136 °E~137 °E locates south of 32 °N;
(4) Others.

According to aforementioned criteria, the number of Kuroshio's nNLM, oNLM, and tLM is 232 (23.4%), 328 (32.9%), and 36 (3.8%), respectively. The averaged position of each type of Kuroshio is illustrated in Fig.1b. On the other hand, the number of others including the transitions among three types of Kuroshio paths is 395 (39.9%), which is beyond the scope of this study.

3. Ocean response to the changes in Kuroshio paths south of Japan

3.1. Spatial distributions of EKE, potential vorticity, and relative vorticity

Before doing the composites for each Kuroshio path, a 5-week running mean is applied to the weekly time-series EKE to eliminate the impact of the synoptic scale. Then the composite is calculated for each Kuroshio path. Note that the time-mean approach used here is simple. Other methods with more physical basis, such as the Multiscale Window Transform (MWT) (Liang and Anderson, 2007; Liang and Robinson, 2009; Liang, 2016), may provide more robust filtered result for the time-mean calculation. Fig. 2 depicts the spatial distribution of averaged EKE for each type of Kuroshio path. It is shown that, when the Kuroshio path is in the nNLM state, there are two significant maxima locating at the east of Kyushu and Kii Peninsulas, respectively (Fig. 2a). The centers appear at the near-shore side of the Kuroshio axis. When the Kuroshio path is in the oNLM or tLM state, however, a maximum locates at the east of Kii Peninsula (Figs. 2b and 2c). The difference between them is that the center distributes along the Kuroshio axis for the tLM state. Furthermore, the maximum of EKE of tLM is larger than those of nNLM and oNLM.

In addition to the EKE associated with variation of Kuroshio path, the PV is also modulated by the variation of western boundary currents, such as Kuroshio and Gulf Stream (e.g., Bower et al., 1985; Leaman et al., 1989; Chen et al., 1992). By analyzing data from shipboard acoustic Doppler current profiler and conductivity-temperature-depth (CTD) profile, Bower (1989) and Oka and Kawabe (2003) have discussed the relationship between PV and western boundary currents. They pointed out PV varies with the path of western boundary currents and the maximum PV locates at the onshore side. The PV at the surface layer is discussed in this study. To obtain the vertical gradient of potential density, the Isshii's subsurface temperature and salinity are used. The information of potential density and surface layer thickness are listed in Table 1. Note that the estimation of PV in this study may not be completely accurate, but it can provide us a heuristic image on the relationship between the PV distribution and the Kuroshio path south of Japan. The spatial distributions of PV of the three types of Kuroshio path are depicted in Fig. 3. Consistent with previous studies, the maximum PV locates at the onshore side of each Kuroshio path. No matter which path Kuroshio takes, moreover, the PV demonstrates a similar distribution along the Kuroshio path. The positive and negative PV locate at the onshore and offshore sides of Kuroshio path, respectively. On the other hand, a maximal center of PV appears at the onshore side of meander path in the south of Honshu, for the cases of oNLM and tLM (Figs. 3b and 3c). Moreover, the tLM has a larger PV than that of oNLM.

It is well-known that relative vorticity relates to the ocean circulation. In general, a decrease in relative vorticity induces a

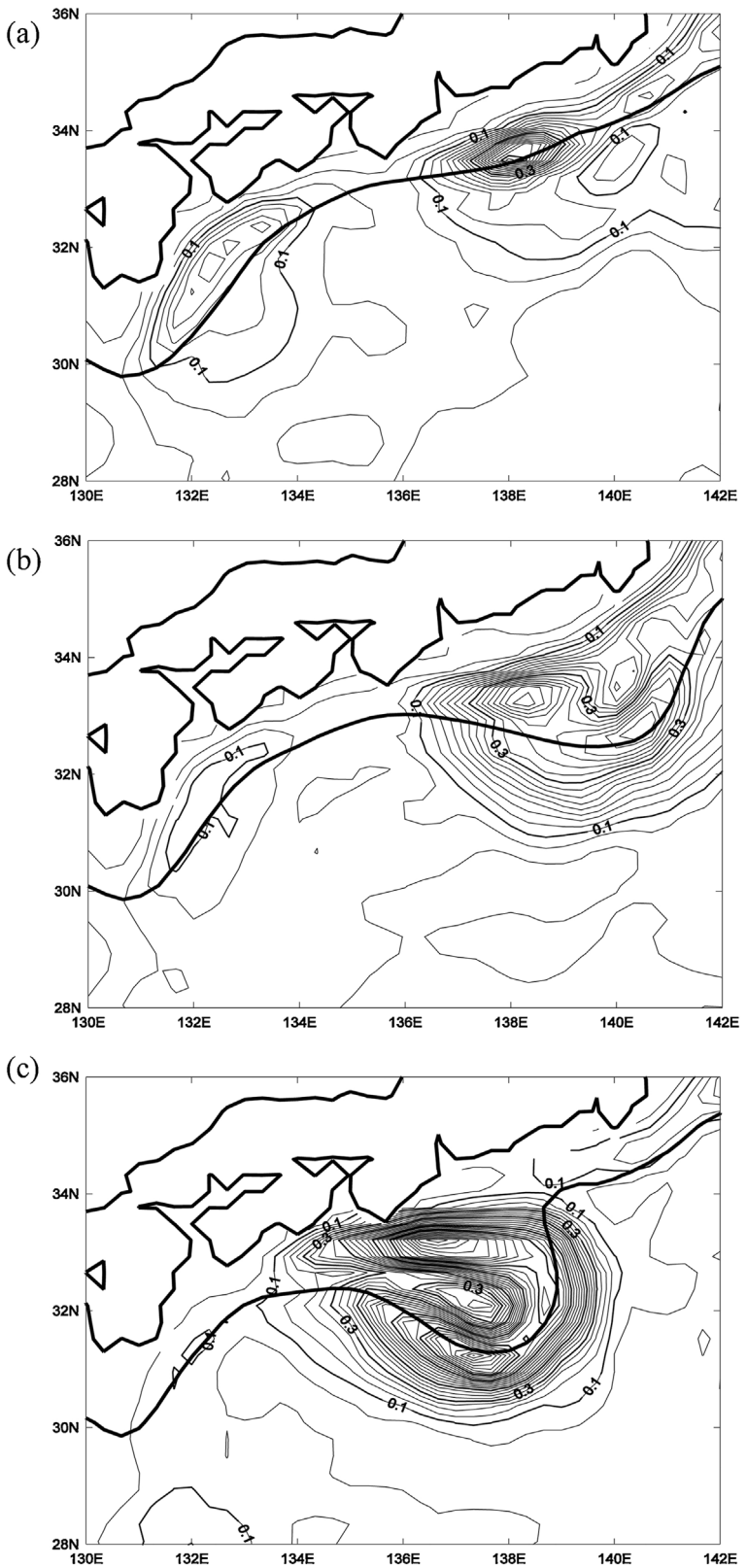

Fig. 2. Spatial patterns of mean eddy kinetic energy ($m^2\ s^{-2}$) of (a) nNLM (CI = 2.5×10^{-2}), (b) oNLM (CI = 2.5×10^{-2}), and (c) tLM (CI = 5.0×10^{-2}). The bold black curves in (a), (b), and (c) show the nNLM, oNLN, and tLM paths, respectively.

Table 1
Parameter values of the region of 130°~140 °E and 24°~32 °N. The reference latitude for f_0 and β_0 is at 30 °N; the other parameter values are derived from Ishii's *T-S* data.

Parameter	nNLM phase	oNLM phase	tLM phase
f_0	7.29×10^{-5} s^{-1}	7.29×10^{-5} s^{-1}	7.29×10^{-5} s^{-1}
β	1.98×10^{-11} m^{-1} s^{-1}	1.98×10^{-11} m^{-1} s^{-1}	1.98×10^{-11} m^{-1} s^{-1}
H_1	100 m	100 m	100 m
H_2	200 m	200 m	200 m
U_1	-0.53 cm s^{-1}	-1.19 cm s^{-1}	-0.30 cm s^{-1}
U_2	-1.50 cm s^{-1}	-2.23 cm s^{-1}	-1.46 cm s^{-1}
ρ_1	$23.32\sigma_\theta$	$23.52\sigma_\theta$	$23.36\sigma_\theta$
ρ_2	$24.91\sigma_\theta$	$24.89\sigma_\theta$	$24.92\sigma_\theta$
ρ_3	$26.99\sigma_\theta$	$27.01\sigma_\theta$	$26.98\sigma_\theta$
γ	0.77	0.65	0.75
$U_1 - U_2$	0.97 cm s^{-1}	1.05 cm s^{-1}	1.16 cm s^{-1}

clockwise circulation. Fig. 4 shows the mean of anomalous relative vorticity of nNLM, oNLM, and tLM. When the Kuroshio path is in the nNLM state, as shown in Fig. 4a, a negative anomalous relative vorticity appears at the east of Kyushu and its center locates along the Kuroshio axis. Furthermore, on the east of Kii Peninsula, there is a negative anomalous relative vorticity on the near-shore side of the Kuroshio axis, whereas a positive anomalous relative voriticity locates off-shore side of the Kuroshio axis. As to the Kuroshio path takes oNLM state, anomalous relative vorticity mainly distributes at the southeast of Kii Peninsula with positive signal along the coast and negative (positive) signal on the near-shore (off-shore) side of the Kuroshio axis (Fig. 4b). Compared to oNLM, tLM has a similar pattern of relative vorticity (Fig. 4c). The difference is the center of negative relative vorticity locates more westward. As discussed above, there is a pair of negative and positive patterns of relative vorticity appear at both sides of a Kuroshio axis. It should be noted that distributions of anomalous relative vorticity of nNLM, oNLM, and tLM are consistent with those of anomalous sea surface height (Fig. 5).

3.2. Interaction between the eddy field and mean flow

It is demonstrated by previous studies that mesocale eddies play a central role in the variability of Kuroshio path south of Japan (e.g., Akitomo and Kurogi, 2001; Endoh and Hibiya, 2001; Mitsudera et al., 2001; Miyazawa et al., 2004). Moreover, eddies also impose significant influence on the volume transport of Kuroshio and zonal migration of Kuroshio path at the east of Taiwan (e.g., Yan et al., 2016; Chang et al., 2018). Thus, to determine whether there is an interaction between the eddy field and mean flow, the climatology of surface ocean currents and anomalous SSH of nNLM, oNLM, and tLM are firstly addressed. Regarding the nNLM, there is a negative center of sea surface height anomaly (SSHA) across the Kuroshio axis at the east of Kyushu (Fig. 5a). At the south of Honshu, there is a pair of eddies with a cyclonic eddy on the onshore side and an anticyclonic eddy on the offshore side of the Kuroshio axis. The cases of oNLM and tLM are different. A cyclonic eddy crosses the meander path at the south of Honshu in the situations of oNLM and tLM (Fig. 5b and c). Meanwhile, the antiyclonic eddies locate at the southwest and northeast sides of the cyclonic eddy. Moreover, the cyclonic and anticylonic eddies of tLM are stronger than those of oNLM. This suggests that the interaction between the eddy field and the mean flow occurs and varies with the variations of the Kuroshio path.

How the eddy-mean flow interaction reacts to the changes in the Kuroshio path? During the last several decades, the rate of barotropic energy conversionis used to interpret this scientific issue (e.g., Lorenz, 1955; Harrison and Robinson, 1978). Based on the 1.5-layer quasi-strophic model, one of its representations is derived for the wind-driven circulation (Berloff and Meacham, 1998), which is already used to study the energetics of Brazil current (Oliveira et al., 2009) and the Kuroshio south of Japan (Ma and Wang, 2014). However, it is also pointed out that the traditionally transport-transfer separation derived from the Reynolds decomposition is not adequately to represent the exact situation (e.g., Holopainen, 1978). Starting from the transformed Eulerian-mean system, Plumb (1983) proposed an alternative scheme, which directly presents the eddy-mean interaction. On the other hand, Liang (2016) derived a unique scheme using the MWT framework (Liang and Anderson, 2007). It takes the following form (see Liang and Anderson, 2007; Liang, 2016 for details):

$$BT = \frac{1}{2}\left[\overline{u_g}\left(\frac{\partial \overline{u_g' u_g'}}{\partial x} + \frac{\partial \overline{u_g' v_g'}}{\partial y}\right) + \overline{v_g}\left(\frac{\partial \overline{u_g' v_g'}}{\partial x} + \frac{\partial \overline{v_g' v_g'}}{\partial y}\right) - \overline{u_g' u_g'}\frac{\partial \overline{u_g}}{\partial x} - \overline{u_g' v_g'}\left(\frac{\partial \overline{u_g}}{\partial y} + \frac{\partial \overline{v_g}}{\partial x}\right) - \overline{v_g' v_g'}\frac{\partial \overline{v_g}}{\partial y}\right] \tag{5}$$

where BT is the rate of barotropic energy conversion, $\overline{u_g' u_g'}$, $\overline{u_g' v_g'}$, and $\overline{v_g' v_g'}$ are the Reynolds stresses. The above BT is the special form of that in Liang (2016), which is the form the Eqs. (14)–(15) in Xu and Liang (2017). Before doing the multiplication, a 5-week running mean is applied to the Reynolds stresses to eliminate the influence of synoptic scale. Then composition is calculated for each type of Kuroshio path. Negative BT represents the energy is transferred from the eddy field to the mean flow, and positive BT represents the energy is transferred from the mean flow to the eddy field.

The distributions of BT of nNLM, oNLM, and tLM are shown in Fig. 6. It is demonstrated that BT varies with the Kuroshio path. tLM has the strongest energy conversion between the eddy field and the mean flow. In general, there is a maximum BT at the south or southeast of Kii peninsula, suggesting the eddy filed extracts energy from the mean flow. When Kuroshio is in the nNLM state, the

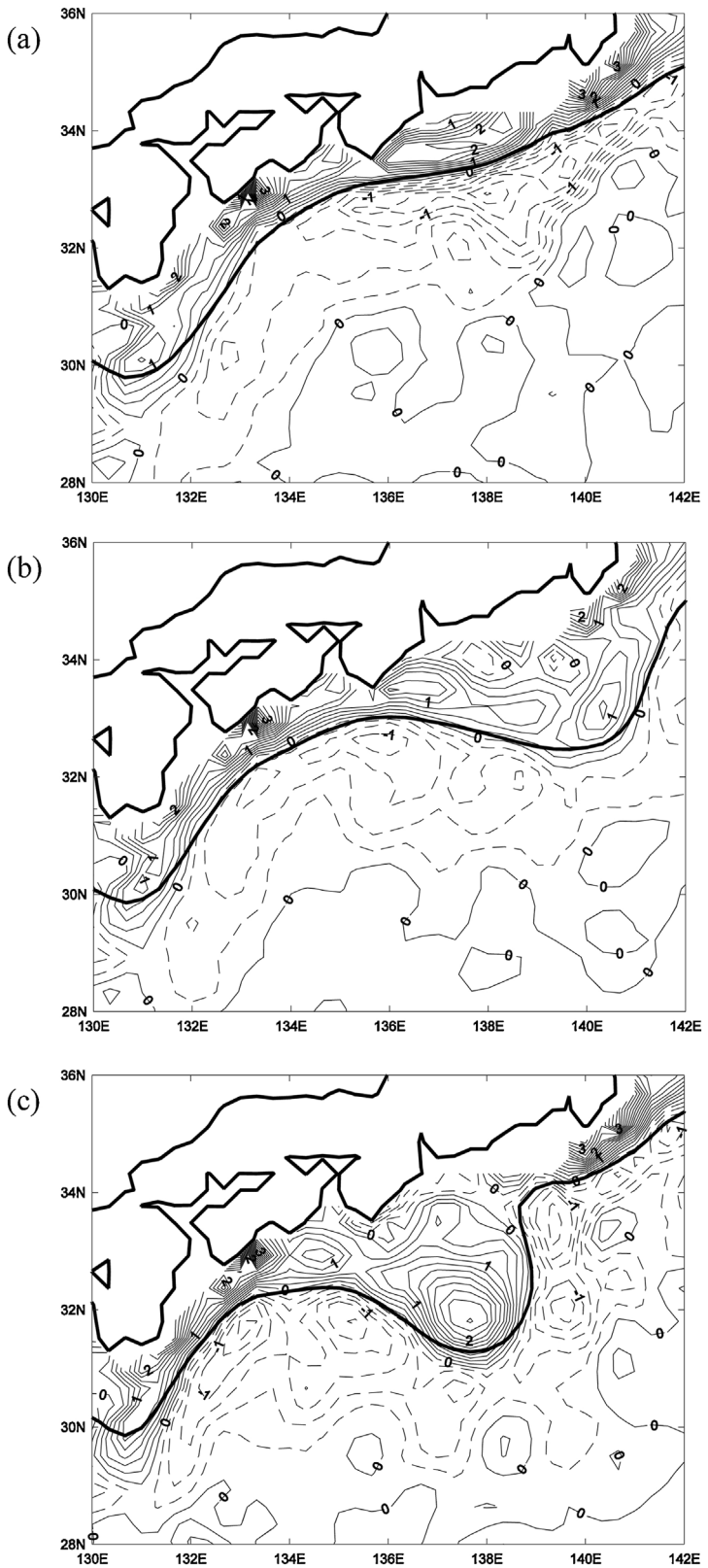

Fig. 3. Spatial patterns of mean potential vorticity (10^{-12} cm^{-1}s^{-1}; CI = 0.25 × 10^{-12}) during (a) nNLM, (b) oNLM, and (c) tLM. The bold black lines in (a), (b), and (c) show the nNLM, oNLN, and tLM paths, respectively.

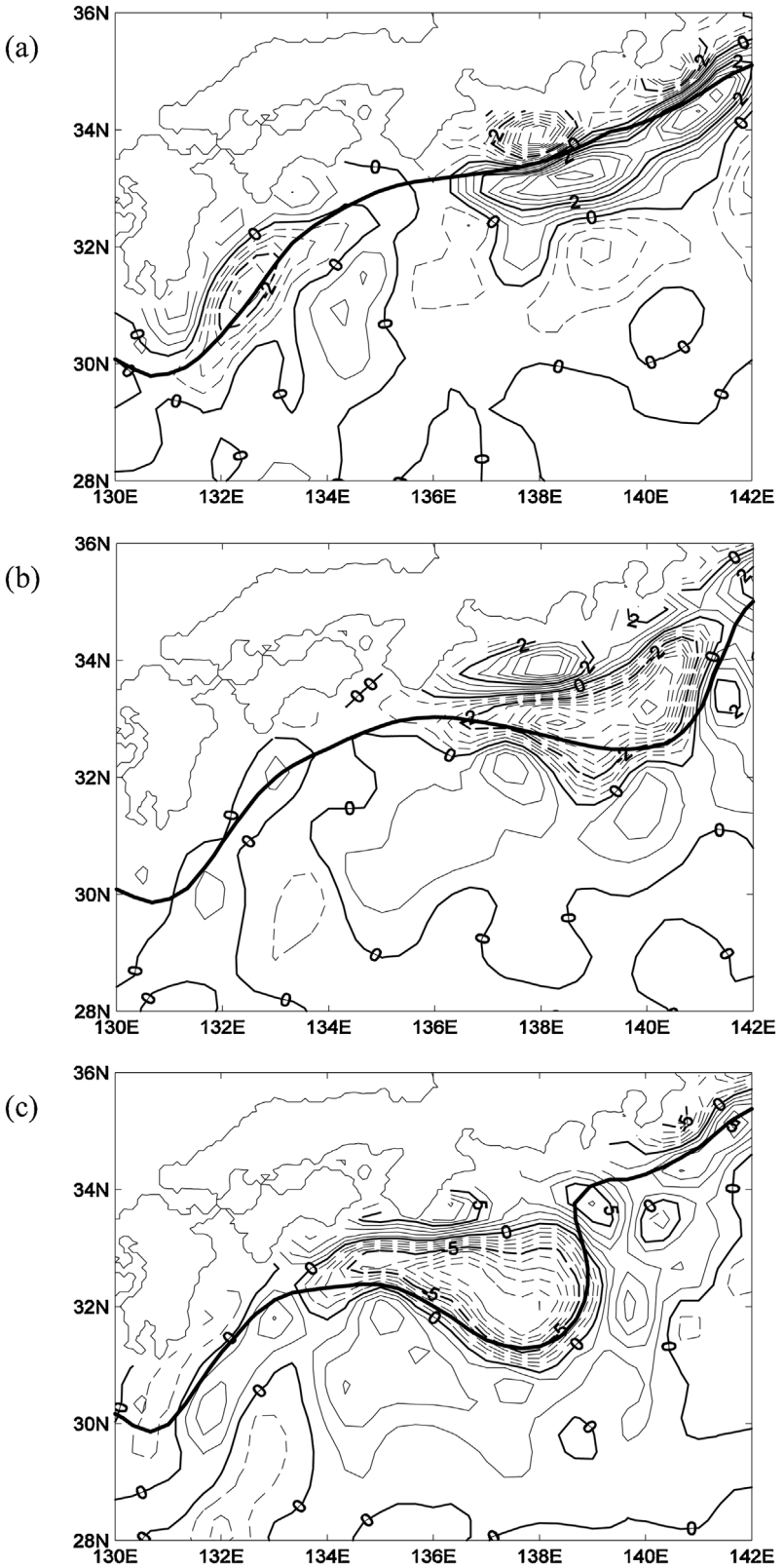

Fig. 4. Spatial patterns of mean state of anomalous relative vorticity of (a) nNLM (CI = 0.5×10^{-6} s^{-1}), (b) oNLM (CI = 0.5×10^{-6} s^{-1}), and (c) tLM (CI = 1×10^{-6} s^{-1}). The bold black lines in (a), (b), and (c) show the nNLM, oNLN, and tLM paths, respectively.

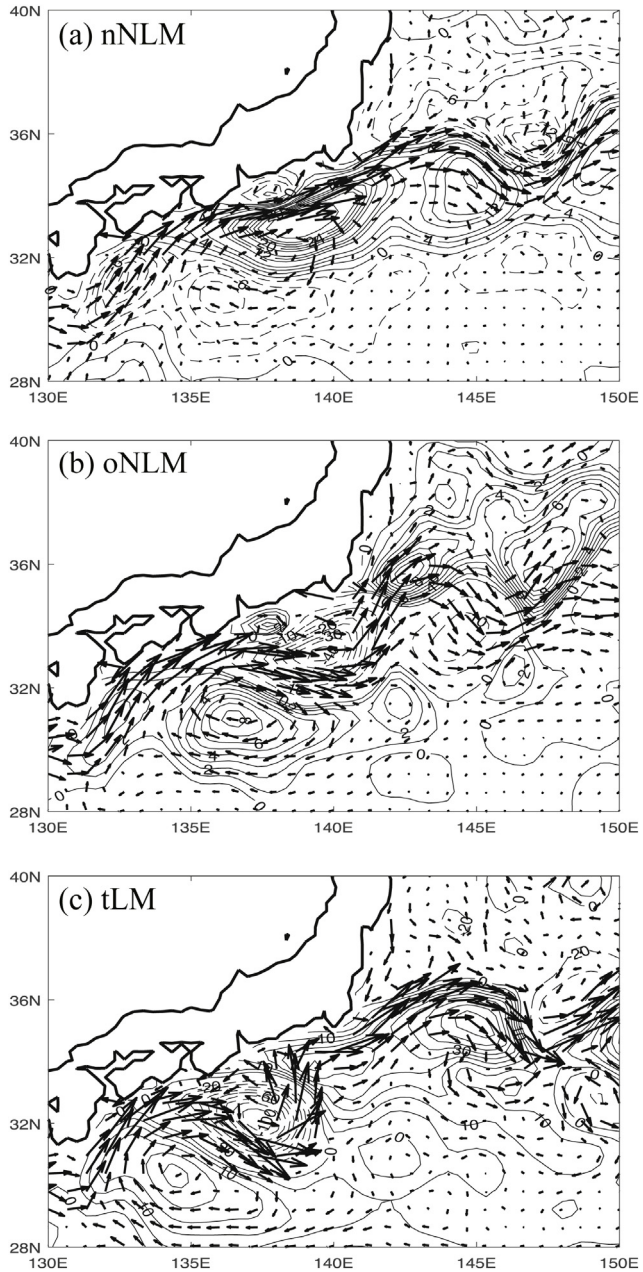

Fig. 5. Mean state of surface geostrophic current (vectors; m/s) and sea surface height anomaly (contours; cm) of (a) nNLM, (b) oNLM, and (c) tLM. Solid and dashed contours represent the postive and negative SSHA, respectively.

positive *BT* at the southeast of Kii peninsula centers at the Kuroshio path, accompanying a negative *BT* at its east side (Fig. 6a). Furthermore, the negative *BT* is also appeared at the south of Shikoku, implying that the mean flow extracts energy from the eddy field. There is a similar distribution of *BT* when Kuroshio takes the oNLM path compared to the nNLM path, but with weaker energy transfer from the eddy field to the mean flow (Fig. 6b). Regarding the tLM path, the energy exchange between the mean flow and the eddy field is largely enhanced compared to both oNLM and nNLM. As shown in Fig. 6c, the center of positive *BT* moves westward, which makes the eddy field extracts energy from the mean flow at the south of Shikoku and Kii peninsula. On the other hand, a negative BT appears along the downstream of the large meander, suggesting the energy is transferred from the eddy field to the mean flow (Fig. 6c). It is possibly implying that the mean flow extracts energy from eddy field at downstream of the meander to maintain the Kuroshio path taking the tLM path.

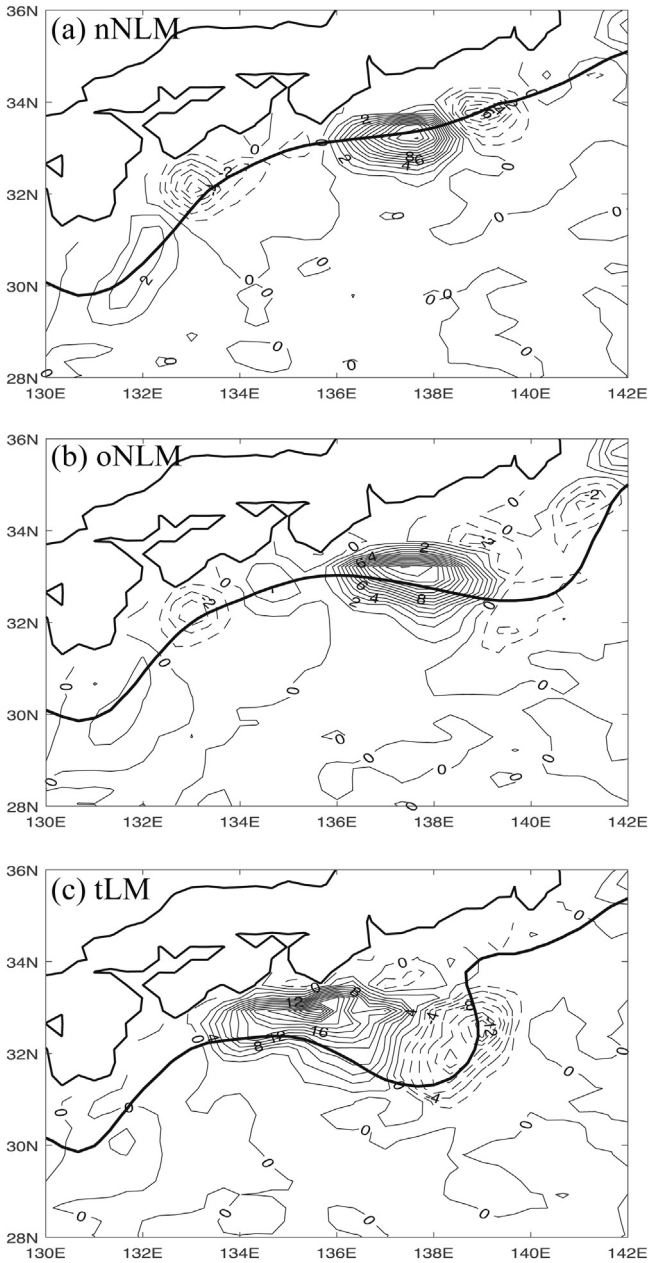

Fig. 6. Spatial patterns of barotropic energy conversion rate (10^{-7} m^2/s^3) of (a) nNLM, (b) oNLM, and (c) tLM. The bold black lines in (a), (b), and (c) show the nNLM, oNLN, and tLM paths, respectively. Solid and dashed contours represent the positive and negative barotropic energy conversion rate, respectively.

3.3. Stability of ocean currents response to changes in Kuroshio paths

In this subsection the stability of current system is discussed by analyzing Ishii's subsurface temperature and salinity data. Based on the classification of Kuroshio paths south of Japan, three cases, representing the nNLM, oNLM, and tLM paths, are selected. The corresponding periods of the three cases are from July 2002 to February 2003, from October 2008 to July 2009, and from July 2004 to April 2005 for nNLM, oNLM, and tLM, respectively. Before discussing the stability, hydrological characteristics of three phases of Kuroshio path are illustrated. Fig. 7 plots the distributions of temperature, vertical gradient of temperature, potential density and zonal component of geostrophic flow along 137 °E. The zonal component of geostrophic flow U_g is estimated by the thermal-wind relationship:

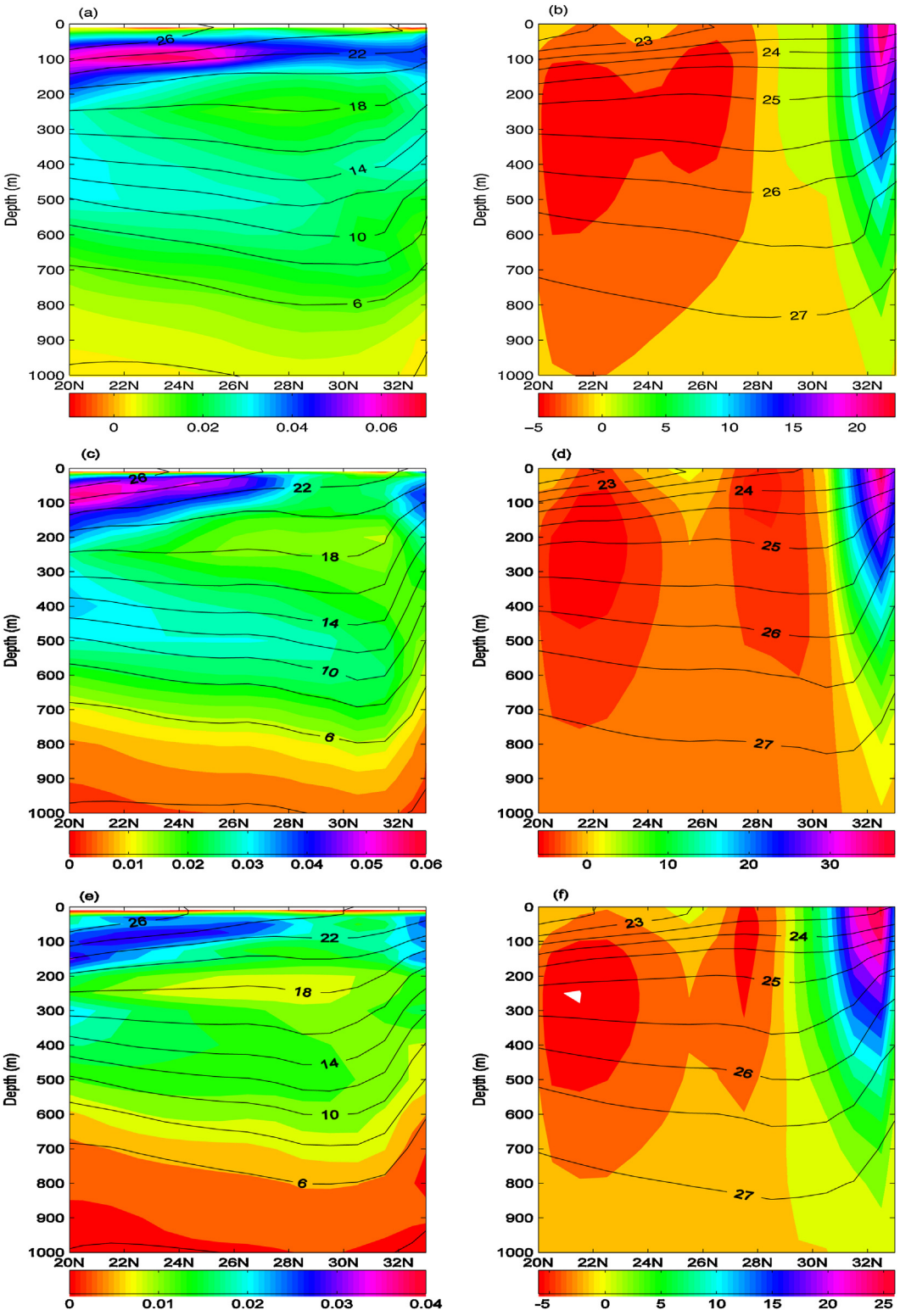

Fig. 7. Depth-latitude plots of temperature (vertical gradient of temperature) (left panel) and density (zonal component of geostrophic velocity) during (a-b) nNLM phase, (c-d) oNLM phase, and (e-f) tLM phase.

$$f\frac{\partial U_g}{\partial z} = \frac{g}{\rho_0}\frac{\partial \rho}{\partial y} \tag{6}$$

where ρ_0 the reference of water density, ρ is the potential density. Furthermore the 1500-m depth is chosen as a reference when calculating U_g.

The three Kuroshio paths, nNLM, oNLM, and tLM, have different hydrological distributions. These three paths have demonstrated isotherms ventilate from the ocean interior to the sea surface, but at different locations (Fig. 7a, c, and e). Take the 24 °C isotherm as an example: it ventilates more northward in nNLM; whereas it ventilates more southward in oNLM. Compared to nNLM and tLM, oNLM has the steepest distribution of isotherms north of 30 °N. Moreover, the isopycnals have a similar distribution as isotherms, especially north of 30 °N (Fig. 7b, d, and f). The ventilation of isotherms and isopycnals induces a significantly horizontal pressure-gradient force there. On the other hand, nNLM has the biggest vertical temperature gradient in the upper 200 m; whereas tLM has the smallest vertical temperature gradient. Additionally, tLM has a local minimal vertical temperature gradient at a depth of 250 m from 23 °N to 30 °N. In addition to temperature and potential density, the zonal component of geostrophic flow also shows different distributions (Fig. 7b, d, and f).

Based on aforementioned discussions, the current system south of Japan may have different stable condition for each type of Kuroshio path. In order to further explore it, a methodology applying the 2.5-layer reduced-gravity model governed by the quasi-geostrophic equation is used (Qiu, 1999), which is already used to discuss the stability of other dynamical systems, like the South Pacific Ocean (Qiu and Chen, 2004) and North Pacific Subtropical Countercurrent (STCC) (Kobashi and Kawamura, 2002; Qiu and Chen, 2010b). This model has two active layers and one unlimited stationary layer. Starting from the reduced-gravity model, we can obtain the following dispersive relation and unstable condition:

$$c^2 - \left(U_1 + U_2 - \frac{P+Q}{R}\right)c + \left(U_1U_2 + \frac{\Pi_1\Pi_2}{R} - \frac{U_1P}{R} - \frac{U_2Q}{R}\right) = 0 \tag{7}$$

and

$$U_1 - U_2 - \gamma U_2 > \gamma\lambda^2\beta \tag{8}$$

where P, Q, and R are the functions of k, l, δ, and λ (refer to Qiu (1999) for the details). If the Eq. (8) is satisfied, the system becomes unstable. Thus, according to the dispersive relation of wave speed c ($c = c_r + ic_i$), we can estimate the increase rate of unstable waves for each Kuroshio path south of Japan. Limited by the ocean bottom topography, the region [130 °E-140 °E] and [22 °N-30 °N] is selected as the study area. On the other hand, the vertical gradient of temperature reaches its maximum at the upper 100 m, and it has a local minimum in the range of 200~300 m (Fig. 7a,c, and e). Thus, the parameter H_1 and H_2 are set to 100 m and 200 m, respectively. Moreover, other corresponding parameters are estimated by Ishii's subsurface temperature and salinity data. These parameters are averaged over the research area (Table 1).

Each Kuroshio path has its own intrinsic ocean properties. As illustrated in Fig. 8, first of all, the current systems of the three Kuroshio paths are all unstable ($c_i \neq 0$). However, they have different increasing rate and time scales of the strongest unstable waves. The increasing rates of the strongest unstable wave of nNLM, oNLM, and tLM are 0.009 day^{-1}, 0.012 day^{-1}, and 0.011 day^{-1}, respectively. The corresponding time scales are 110 days, 80 days, and 90 days. Moreover, among the three Kuroshio paths, the oNLM has the biggest admissive window of unstable waves; whereas nNLM has the smallest admissive window of unstable waves. On the other hand, strong vertical velocity shear ($U_1 - U_2$) and weak stratification (γ) will cause strong baroclinic instability (Qiu, 1999; Jia et al., 2011). As the numbers show in Table 1, the vertical velocity shear of nNLM, oNLM, and tLM paths are 0.97 cm s^{-1}, 1.05 cm s^{-1}, and 1.16 cm s^{-1}, respectively. While the stratification of nNLM, oNLM, and tLM paths are 0.77, 0.65, and 0.75, respectively. It is shown that the oNLM and tLM paths have larger vertical velocity shear and smaller stratification compared to the nNLM path, implying that both oNLM and tLM paths have stronger baroclinic instability than that of the nNLM path.

4. Summary and discussion

Based on the satellite altimeter from AVISO and Ishii's subsurface temperature and salinity data, the response of ocean dynamics, in terms of the EKE, relative vorticity, eddy-mean flow interaction, and stability of ocean currents, to the Kuroshio path south of Japan is discussed. Results reveal that the centers of EKE appear at the near-shore side of the Kuroshio axis. When the Kuroshio path is in the oNLM or tLM state, a maximum EKE locates at east of Kii Peninsula. The difference between them is that the center distributes along the Kuroshio axis. Furthermore, tLM has the largest maximum EKE among all. The EKE calculated in this study is estimated by taking averages over the quadratic products of the eddy fields. However, it should be pointed out that this calculation has some limitation for the nonstationary processes. Methods with more physical basis, such as the MWT, may conquer such limitation and provide more robust results for the nonstationary processes.

Consistent with previous studies, the maximum PV of nNLM, oNLM, and tLM appears at the onshore side of Kuroshio axis. The negative PV varies along the Kuroshio axis at the offshore side. The spatial distributions of relative voritcity resemble those of EKE. When Kuroshio takes the nNLM path, there is a negative anomalous relative vorticity centering along the path at the east of Kyushu. The negative and positive relative vorticity appear at the north and south of the Kuroshio path south of Honshu. Regarding the oNLM path, it has a triple structure at the south of Honshu which is the negative relative vorticity, locating at the center, with the positive relative vorticity at both the onshore and offshore sides of it. The difference between oNLM and tLM is that the center of negative relative vorticity of oNLM locates more westward. On the other hand, the distributions of the relative vorticity of nNLM, oNLM, and

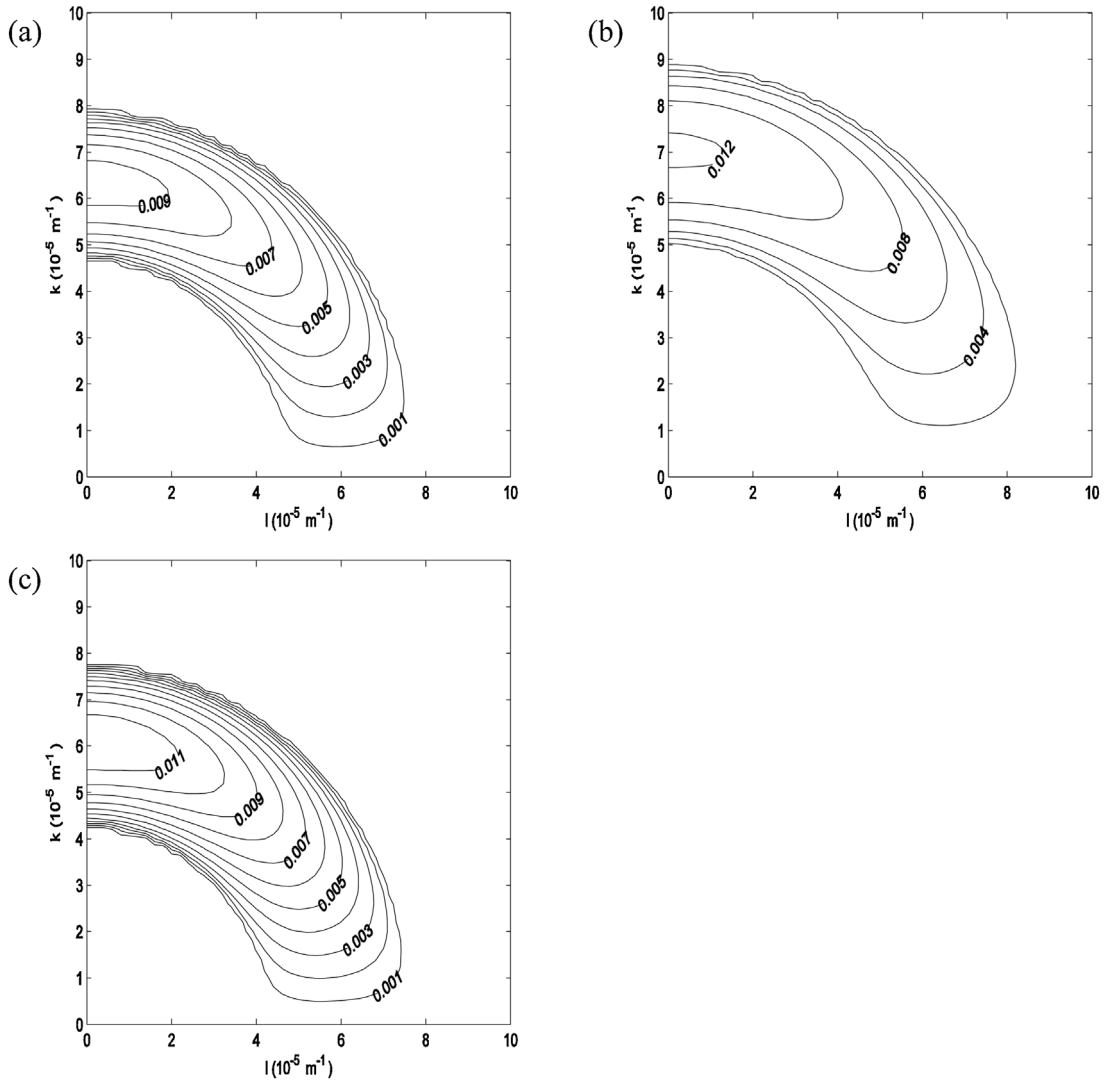

Fig. 8. Growth rate (day^{-1}) of the unstable waves as a functions of zonal and meridional wavenumber during (a) nNLM phase, (b) oNLM phase, and (c) tLM phase.

tLM are consistent with those of SSHA.

In terms of the rate of barotropic energy conversion, the eddy-mean flow interaction shows diverse structures among the three Kuroshio paths. Compared to nNLM and oNLM, tLM has the most intensified energy exchange between eddy field and the mean flow. Regarding the tLM path, the role of eddy field in the upstream south of Honshu is extracting energy from the mean flow and weakening the mean flow. On the other hand, the eddy field works on the mean flow and strengthens the mean flow at the downstream of tLM south of Honshu, possibly favoring the Kuroshio keeps its path. Moreover, stability analysis of the current system shows that each Kuroshio path has its own intrinsic ocean condition. Results illustrate the current systems of the three Kuroshio paths are unstable, but they have different increasing rates and time scales of the strongest unstable waves. oNLM has the biggest admissive window of unstable waves; whereas nNLM has the smallest admissive window of unstable waves. On the other hand, smaller stratification and larger vertical velocity shear suggest that oNLM and tLM have stronger baroclinic instability compared to the nNLM path.

The primary results presented in this study are obtained from the satellite SSH and reanalysis data. It needs further discussion by using model results and in situ observation data (e.g., Argo float and CTD). On the other hand, the analysis illustrated in the study reveals that the Kurhshio paths south of Japan have their ocean dynamic conditions and properties. These may lead to different atmospheric response to each Kuroshio path. Xu et al. (2010) discussed the impacts of the tLM path occurred in 2004-2005 on the atmosphere by analyzing results of a regional atmosphere model. They addressed that the cool pool of sea surface temperature (SST) south of Honshu slowes down the wind speed and reduces the precipitation. However, the oNLM path also accompanies a cool SST pool south of Honshu. Will any different atmospheric response happens? Does the cool SST pool associate with oNLM path cause

significant changes in the atmosphere? These topics need further investigation.

Acknowledgements

The author appreciates the significant suggestions and comments from three anonymous reviewers. The author also thanks Dr. Xiao Zhang for her comments and language editing. This study is sponsored by the Nanjing University of Information Science and Technology through funding of the joint China-US Atmosphere-Ocean Research Center at the University of Hawaii at Manoa, and the project funded by the Priority Academic Program Development of Jiangsu Higher Education Institutions (PAPD). This study is also funded by the Startup Foundation for Introducing Talent of NUIST (No. 2018r064/2241011801064). This is the SOEST publication number 10623, the IPRC publication number 1356, and the ESMC publication number 246.

References

Akitomo, K., Kurogi, M., 2001. Path transition of the Kuroshio due to mesoscale eddies: a two-layer, wind-driven experiment. J. Oceanogr. 57, 735–741.
AVISO, 2008. SSALTO/DUCAS User Handbook: (M)SLA and (M)ADT Near-real Time and Delayed Time Products. Aviso Altimetry, Ramonville St. Agne, France 32p.
Berloff, P., Meacham, S.P., 1998. On the stability of the wind-driven circulation. J. Mar. Res. 56, 937–993.
Bower, A., 1989. Potential vorticity balances and horizontal divergence along particle trajectories in Gulf Stream meanders east of Cape Hatteras. J. Phys. Oceanogr. 19, 1669–1681.
Bower, A., Rossby, H., Lillibridge, J., 1985. The Gulf Stream-Barrier or blender? J. Phys. Oceanogr. 15, 24–32.
Chang, M., Jan, S., Mensah, V., Andres, M., Rainville, L., Yang, Y., Cheng, Y., 2018. Zonal migration and transport variations of the Kuroshio east of Taiwan induced by eddy impingements. Deep-sea Res. 131 (Part I), 1–15.
Chen, C., Beardsley, R., Limeburner, R., 1992. The structure of the Kuroshio southwest of Kyushu: velocity, transport and potential vorticity fields. Deep-sea Res. 39, 245–268.
Ducet, N., Le Traon, P.Y., Reverdin, G., 2000. Global high-resolution mapping of ocean circulation from TOPEX/Poseidon and ERS-1 and -2. J. Geophys. Res. 105, 19477–19498.
Ebuchi, N., Hanawa, K., 2000. Mesoscale eddies observed by TOLEX-ADCP and TOPEX/POSEIDON altimeter in the Kuroshio recirculation region south of Japan. J. Oceanogr. 56, 43–57.
Ebuchi, N., Hanawa, K., 2003. Influences of mesoscale eddies on variations of the Kuroshio path south of Japan. J. Oceanogr. 59, 25–36.
Endoh, T., Hibiya, T., 2001. Numerical simulation of the transient response of the Kuroshio leading to the large meander formation south of Japan. J. Geophys. Res. 106, 26833–26850.
Hall, M.M., 1991. Energetics of the Kuroshio Extension at 35°N, 152°E. J. Phys. Oceanogr. 21, 958–975.
Harrison, D.E., Robinson, A.R., 1978. Energy analysis of open regions of turbulent flows – Mean eddy energetics of a numerical ocean circulation experiment. Dyn. Atmos. Oceans 2, 185–211.
Hayasaki, M., Kawamura, R., Mori, M., Watanabe, M., 2013. Response of extratropical cyclonic activity to the Kuroshio large meander in northern winter. Geophy. Res. Lett. 40, 2851–2855.
Holopainen, E.O., 1978. A diagnostic study on the kinetic energy balance of the long-term mean flow and the associated transient fluctuations in the atmosphere. Geophysica 15, 125–145.
Ishii, M., Kimoto, M., Kachi, M., 2003. Historical ocean subsurface temperature analysis with error estimates. Monthly Weather Review 131, 51–73.
Ishii, M., Kimoto, M., Sakamoto, K., Iwasaki, S.I., 2006. Steric sea level changes estimated from historical ocean subsurface temperature and salinity analyses. J. Oceanogr 62, 155–170.
Ishii, M., Shouji, A., Sugimoto, S., Matsumoto, T., 2005. Objective analyses of SST and marine meteorological variables for the 20th century using COADS and the Kobe Collection. Int. J. Climatol. 25, 865–879.
Jia, F., Wu, L., Qiu, B., 2011. Seasonal modulation of eddy kinetic energy and its formation mechanism in the southeast Indian Ocean. J. Phys. Oceanogr. 41, 657–665.
Kawabe, M., 1995. Variations of current path, velocity, and volume transport of the Kuroshio in relation with the large meander. J. Phys. Oceanogr. 25, 3103–3117.
Kobashi, F., Kawamura, H., 2002. Seasonal variation and instability nature of the North Pacific subtropical countercurrent and the Hawaiian Lee countercurrent. J. Geophys. Res. Ocean 107. https://doi.org/10.1029/2001JC001225.
Leaman, K., Johns, E., Rossby, T., 1989. The average distribution of volume transport and potential vorticity with temperature at three sections across the Gulf Stream. J. Phys. Oceanogr. 19, 36–51.
Le Traon, P.Y., Faugere, Y., Hernandez, F., Dorandeu, J., Mertz, F., Ablain, M., 2003. Can we merge GEOSAT Follow-On with TOPEX/Poseidon and ERS-2 for an improved description of the ocean circulation? J. Atmos. Oceanic. Technol. 20, 889–895.
Liang, X.S., 2016. Canonical transfer and multiscale energetic for primitive and quasigeostrophic atmospheres. J. Atmos., Sci. 73, 4439–4468.
Liang, X.S., Anderson, D., 2007. Multiscale window transform. SIAM J. Multiscale Model.Simul. 6, 437–467.
Liang, X.S., Robinson, A., 2009. Multiscale processes and nonlinear dynamics of the circulation and upwelling events off Montery Bay. J. Phys. Oceanogr. 39, 290–313.
Lorenz, E.N., 1955. Available potential energy and the maintenance of the general circulation. Tellus 7, 157–167.
Ma, L.B., 2014. Spatiotemporal features and possible mechanisms of seasonal changes in sea surface height south of Japan. Chinese J. Oceano. Limno. 32, 933–945.
Ma, L.B., Wang, Q., 2014. Interannual Variations in Energy Conversion and Interaction between the Mesoscale Eddy Field and Mean Flow in the Kuroshio South of Japan. Chinese J. Oceano. Limno. 32, 210–222.
Mitsudera, H., Waseda, T., Yoshikawa, Y., Taguchi, B., 2001. Anticyclonic eddies and Kuroshio meander formation. Geophys. Res. Lett. 28, 2025–2028.
Miyamoto, H., Itoh, H., Okazaki, Y., 2017. Temporal and spatial changes in the copepod community during the 1974-1998 spring seasons in the Kuroshio region: a time period of profound changes in pelagic fish populations. Deep-sea Res. Part I 128, 131–140.
Miyazawa, Y., Guo, X.Y., Yamagata, T., 2004. Roles of mesoscale eddies in the Kuroshio paths. J. Phys. Oceanogr. 34, 2203–2222.
Nakamura, H., Nishina, A., Minobe, S., 2013. Response of storm tracks to bimodal Kuroshio path states south of Japan. J. Clim. 25, 7772–7779.
Nakata, K., Hada, A., Matsukawa, Y., 1994. Variations in food abundance for Japanese sardine larvae related to the Kuroshio meander. Fish. Oceanogr. 3, 39–49.
Oka, E., Kawabe, M., 2003. Dynamic structure of the Kuroshio south of Kyushu in relation to the Kuroshio path variations. J. Oceanogr. 59, 595–608.
Oliveira, L., Piola, A., Mata, M., Soares, I., 2009. Brazil current surface circulation and energetics observed from drifting buoys. J. Geophys. Res. 114. https://doi.org/10.1029/2008JC004900.
Plumb, R.A., 1983. A new look at the energy cycle. J. Atmos. Sci. 40, 1669–1688.
Qiu, B., 1999. Seasonal eddy field modulation of the North Pacific Subtropical Countercurrent: TOPEX/Poseidon observations and theory. J. Phys. Oceanogr. 29, 2471–2486.
Qiu, B., Chen, S.-M., 2004. Seasonal modulations in the eddy field of the South Pacific Ocean. J. Phys. Oceanogr. 34, 1515–1527.
Qiu, B., Chen, S.-M., 2005. Variability of the Kuroshio Extension jet, recirculation gyre, and mesoscale eddies on decadal time scales. J. Phys. Oceanogr. 35, 2090–2103.
Qiu, B., Chen, S.-M., 2010a. Eddy-mean flow interaction in the decadally modulating Kuroshio Extension system. Deep-sea Res.-II 57, 1098–1110.
Qiu, B., Chen, S.-M., 2010b. Interannual variability of the North Pacific Subtropical Countercurrent and its associated mesoscale eddy field. J. Phys. Oceanogr. 40, 213–225.

Rio, M., Guinehut, S., Larnicol, G., 2011. New CNES-CLS09 global mean dynamic topography computed from the combination of GRACE data, altimetry, and in situ measurements. J. Geophy. Res. 116. https://doi.org/10.1029/2010JC006505.
Sugimoto, S., Hanawa, K., 2012. Relationship between the path of the Kuroshio in the south of Japan and the path of Kuroshio Extension in the east. J. Oceanogr. 68, 219–225.
Usui, N., Tsuijno, H., Fujii, Y., Kamachi, M., 2008. Generation of a trigger meander for the 2004 Kuroshio larger meander. J. Geophys. Res. 113. https://doi.org/10.1029/2007JC004266.
Waseda, T., Mitsudera, H., Taguchi, B., Yoshikawa, Y., 2003. On the eddy-Kuroshio interaction: Meander formation process. J. Geophys. Res. 108. https://doi.org/10.1029/2002JC001583.
Xu, F., Liang, X.S., 2017. On the generation and maintenance of the 2012/13 sudden stratospheric warming. J. Atmos. Sci. 74, 3209–3228.
Xu, H.M., Tokinage, H., Xie, S.P., 2010. Atmospheric effects of the Kuroshio Large Meander during 2004-05. J. Clim. 23, 4704–4715.
Yan, X., Zhu, X., Pang, C., Zhang, L., 2016. Effects of mesoscale eddies on the volume transport and branch pattern of the Kuroshio east of Taiwan. J. Geophy. Res. Oceans 121. https://doi.org/10.1002/2016JC012038.
Zhang, Z., Ichikawa, K., 2005. Influence of the Kuroshio fluctuations on sea level variations along the south coast of Japan. J. Oceanogr. 61, 979–985.